

EDDY CURRENT SHIELDING BY ELECTRICALLY THICK VACUUM CHAMBERS*

Boris Podobedov[#], Lynne Ecker, David Harder, George Rakowsky,
BNL, Upton, New York

Abstract

The AC response of accelerator vacuum chambers to external magnetic fields when the wall thickness is comparable or greater than the skin depth was investigated. Good agreement was established between experimental measurements, analytical modelling and finite element simulations. Based on the results we suggest a transfer function model for electrically thick vacuum chambers with arbitrary transverse cross-section.

INTRODUCTION

EM field penetration into accelerator vacuum chambers and its shielding by eddy currents is a well known subject in accelerator physics and engineering. It is commonly encountered in the design of pulsed kicker magnets, ramped magnets, and other magnets designed to create a rapidly changing magnetic field inside a metallic vacuum chamber. Typical calculations include field attenuation, field rise-time, generation of (usually unwanted) multipole components, eddy current heat generation, etc.

In particular, a commonly mentioned model is that of an electrically thin chamber with circular cross-section [1]. It states that for a sinusoidal excitation $B_{ext}(t)=B_0\sin(\omega t)$ applied transversely to a beam pipe of radius b and wall thickness d the steady-state time dependence for the magnetic field penetrating the vacuum chamber $B_{int}(t)$ is:

$$B_{int}(t) = \frac{B_0}{\sqrt{1+(\omega\tau)^2}} \sin(\omega t - \tan^{-1}(\omega\tau)), \quad (1)$$

$$\tau = \frac{1}{2} \mu_0 \sigma_c b d, \quad (2)$$

where σ_c is the conductivity of the chamber material. This corresponds to the Laplace domain transfer function

$$\tilde{B}_{int} / \tilde{B}_{ext} = \frac{1}{1 + p\tau}. \quad (3)$$

Note that in this model the field inside the chamber lags no more than 90 degrees behind the external field.

The present work was motivated by the need to understand the AC magnetic (dipolar) field penetration into the National Synchrotron Light Source (NSLS) vacuum chamber, to allow for better modelling of the orbit feedback systems [2]. While the feedback loop includes many elements, such as corrector power supplies, electron beam, beam position monitors with processing electronics, etc., the dynamic response of the (open loop) system is dominated by the eddy currents in the vacuum chamber. Since the dynamic response to the horizontal and vertical fields was different and phase

shifts greatly exceeding 90 degrees were measured [2], a model based on the equations above is inadequate. This is not too surprising because 1) chambers don't have circular symmetry and 2) they cannot be assumed electrically thin at high excitation frequencies. Earlier papers [3-4] that mention eddy current time constants for accelerator vacuum chambers in non-circular geometry derive them by an order of magnitude estimation, and thus don't provide sufficient accuracy for our application.

The goal of this work was to study the accelerator beam pipe response in a realistic geometry as well as to come up with a simple dynamic model that could quantitatively describe the effects observed.

ANALYTICAL ESTIMATES

An obvious generalization of Eq. (1) is to account for finite wall thickness of the vacuum chamber. For axially symmetric geometry the solution for a long tubular cylinder in a uniform transverse quasi-static magnetic field can be found by standard methods of classical electrodynamics. Eddy currents flow parallel to the cylinder axis, they are strongest at the outer surface, and decay inside the metal due to the skin effect. The field inside the cylinder is uniform. The transfer function is given by

$$\frac{\tilde{B}_{int}}{\tilde{B}_{ext}} = \frac{2/q^2}{I_0(q+qd/b)K_2(q)-I_2(q)K_0(q+qd/b)}, \quad (4)$$

where $q \equiv \sqrt{2p\tau b/d}$, b stands for the inner radius, τ is given by Eq. (2), I and K are the corresponding Bessel functions. Note that parameter qd/b is approximately the ratio of the wall thickness to the skin depth. When this parameter is small we recover the first order transfer function Eq. (3). In general, however, Eq. (4) has infinite number of poles. Their scaling with chamber thickness is illustrated in Fig. 1. Solid curves show exact calculation, while the dashed curves show asymptotic behaviour for vanishing thickness given by $p_0=-1/\tau$ and, for $n=1,2,3,\dots$,

$$p_n = \frac{1}{2} p_0 n^2 \pi^2 b/d = -n^2 \pi^2 / (\mu_0 \sigma_c d^2). \quad (5)$$

Apart from the factor $\pi^2/2$ the poles of Eq. (5) correspond to the frequencies where the skin depth is equal to d/n . Eq. (5) is quite accurate (see Fig. 1). Even for a very thick wall, $d/b=1$, the largest disagreement is less than 30%.

A similar transfer function and pole behaviour can be derived for parallel plate geometry with B_{ext} parallel to the(finite thickness) plates, so it is expected that the relationship between the dominant pole and higher frequency poles will be approximately the same for other vacuum chamber geometries as well.

*Work supported by DOE contract number DE-AC02-98CH10886
#boris@bnl.gov

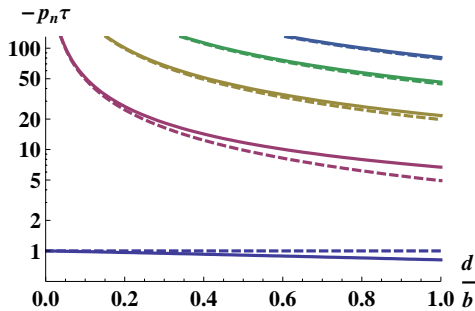


Figure 1: Transfer function poles for a thick tubular cylinder.

However, for more realistic geometries the situation is more complicated since the field inside a chamber generally depends on the transverse position and it has components both parallel and perpendicular to the external field. In other words, the response to a dipolar excitation generally contains higher multipoles of the field. For small orbit displacements it is still useful to introduce the dipolar response transfer function, $\tilde{B}_{\text{int}}(x = y = 0) / \tilde{B}_{\text{ext}}$.

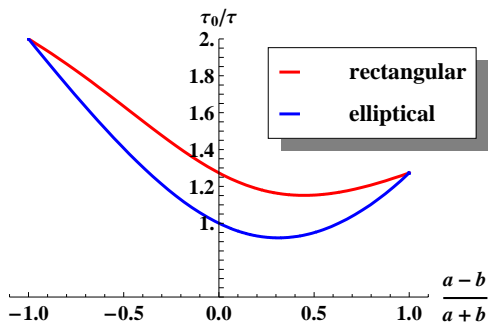


Figure 2: Thin pipe shortest time constant, Eq.(6); semi-axis a is fixed; B_{ext} parallel to semi-axis b .

This function, even for electrically thin chambers, contains infinite number of poles (and zeros), since each multipole mode has an associated time constant, and all modes are coupled. Nevertheless, at low frequencies it could be significantly simplified [7], and cast into a single-pole form similar to Eq.(1), except the pole frequency is now given by

$$p_0^{-1} \equiv \tau_0 = \frac{\mu_0 \sigma_c d}{2\pi} \oint \frac{x^2}{x^2 + y^2} ds. \quad (6)$$

Here we assume symmetric chambers with respect to both $x=0$ and $y=0$ planes. The integral is taken around the transverse chamber cross-section. For instance, for circular chamber, $y/x = \tan \theta$, $ds = b d\theta$, and by integration over the polar angle θ , we recover Eq. (2). Note that expression similar to Eq. (6) follows from Eq. (16) of [5] in the limit of a large magnet gap. That derivation was done by a different method in the limit of weak skin effect (i.e. low frequency) for a thin chamber with mode coupling ignored.

Time constants from Eq. (6) are plotted in Fig. 2. As the cross-section changes (left to right) from parallel plates parallel to B_{ext} , to round (or square), and then to

parallel plates perpendicular to B_{ext} , the time constant changes by roughly a factor of two. For square pipe, $\tau_0/\tau = 4/\pi$, which is the same as for parallel plates perpendicular to B_{ext} .

Combining the dominant pole from Eq. (6) with the ones described earlier for a thick tubular cylinder (and $n > 0$) we suggest the following transfer function model that accounts for non-circular cross-section as well as the wall thickness,

$$\frac{\tilde{B}_{\text{int}}(x = y = 0)}{\tilde{B}_{\text{ext}}} = \frac{p_0 p_1 p_2 \dots}{(p + p_0)(p + p_1)(p + p_2) \dots}. \quad (7)$$

Here p_0 is calculated from Eq.(6) while higher frequency poles are taken from the right hand side of Eq. (5), i.e.

$p_{n>0} = -n^2 \pi^2 / (\mu_0 \sigma_c d^2)$. We note that for most applications accounting for just a few poles in Eq. (7) gives sufficient accuracy. This will be illustrated below.

HALL PROBE AND ANSYS RESULTS

The measurements presented here were a part of a larger task to characterize the dynamic response of the key elements in the NSLS orbit feedback system. Actual NSLS ring hardware (trim magnets, power supplies, beam pipe) were used. Two different types of trim magnets were used: an air-core magnet and an iron-frame magnet. Similar results have been obtained for the chamber response.

The air-core magnet produces only a horizontal field. The iron core magnet has several sets of coils; for the measurements presented only the horizontal coils were powered. The Hall probe was oriented vertically (i.e. sensitive to the horizontal field) and was located at the center of the magnet. The transverse field profile over the area occupied by the pipe was measured (at DC) and field uniformity was found to be at ~10%.

Frequency response measurements were done using a Stanford Research Systems SR785 Dynamic Signal Analyzer. The SR785 output was connected to the current programming input on a Kepco BOP20-10M Bipolar Power Supply operating in constant current mode. A calibrated Allegro A1360 Hall sensor with a 50 kHz bandwidth was inserted on the axis into the bore of the magnet. The setup was arranged so that pipes of different shape and wall thicknesses could be inserted into the bore on the opposite side from the probe insertion. The current sensing amplifier output from the supply was connected to input 1 on the dynamic signal analyzer and the Hall probe signal was connected to input 2. Thus the phase and amplitude relationship between the current through the magnet windings and the magnetic field in the bore of the magnet could be analysed as a function of frequency for different pipe geometries. The photo of the setup is shown in Fig. 3.

Round Pipe Results

To check our assumptions and the measurement technique the AC magnetic field penetration into a pipe of



Figure 3: Measurement setup with air-core magnet.

a circular cross-section was studied. The pipe, made out of aluminium ($\sigma_c=2.7 \times 10^7 (\Omega\text{-m})^{-1}$), had an inner radius $b=19$ mm and thickness $d=4$ mm. It was more than a factor of two longer than the magnet.

Results for this pipe are shown in Fig. 4. Clearly chamber response significantly deviates from the first order system response of Eq. (1), which is especially apparent in the phase curve. The phase lag exceeds 90 degrees at frequencies higher than ~ 280 Hz. On the other hand, the exact analytical expression, Eq. (4) matches the data quite well. Even a rather subtle feature of the change in the sign of the second derivative of the phase is in agreement with the data. If Eq. (4) is replaced by Eq. (7) then 3-4 poles are enough to obtain a similar agreement with the data over this frequency range.

Good agreement for the round pipe suggests that 1) our measurement technique is sound; 2) approximations we make for modelling, such as infinitely long pipe, and uniform external field, are reasonable and 3) the response of accelerator chambers in a more realistic geometry should be modelled in similar manner, with thickness effects included.

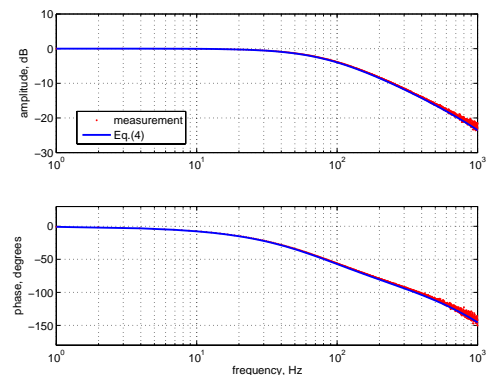


Figure 4: AC response for the pipe with round cross-section.

NSLS Chamber Results

The chamber we measured next (shown in Fig. 3) had a rectangular cross-section with 42×80 mm² inner dimension and $d=4$ mm thickness. It was made from 6061-T4 extruded aluminium. This is a simplified version of the true NSLS vacuum chamber that in addition typically has ante-chamber and/or cooling channels. Results together with Eq. (7) are shown in Fig. 5.

In addition to the measurements, we studied NSLS chamber response with the low-frequency EM field simulator in the finite-element modelling package ANSYS [6]. The 2D model had $\frac{1}{4}$ symmetry ($x>0, y>0$) with standard boundary conditions. A uniform B_{ext} parallel to the x -axis was fixed at 0.5 m radius from the center of the chamber. For frequencies up to 100 Hz five elements through the thickness of the tube were modelled and for higher frequencies ten elements through the thickness of the tube were used to better approximate variations in the field. The more refined model consisted of approximately 94,000 nodes and used PLANE13 ANSYS elements. Amplitude and phase with respect to B_{ext} was extracted from Re and Im components of $B_{int}(x=y=0)$ estimated by the model. Figure 5 shows ANSYS results in green circles. They agree well with the measurements and analytical results.

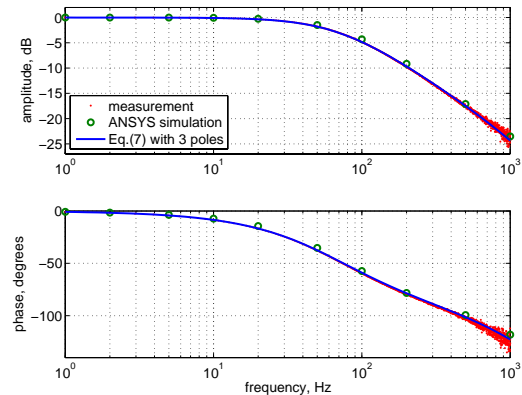


Figure 5: AC response for the NSLS vacuum chamber.

CONCLUSION

We performed Hall probe measurements, finite element simulations and analytical studies of dipolar AC magnetic field penetration into electrically thick vacuum chambers in realistic geometry. Good agreement is observed between all three. In addition our results for NSLS chamber agree with electron beam orbit response measurements performed earlier in the NSLS VUV ring during orbit feedback system commissioning.

More fundamentally we have shown that the chamber response can be well modelled by a simple transfer function, Eq. (7); for most applications it is enough to include only a few poles. Explicit expressions for the poles are given in Eq. (6) and after Eq. (7).

REFERENCES

- [1] A. Chao and M. Tigner, Handbook of Accelerator Physics, World Scientific (1999), p. 125
- [2] B. Podobedov et al, Proceedings PAC-2001, p. 396
- [3] S. Kurennoy, Proceedings PAC-1993, p. 3420
- [4] S. H. Kim, APS note LS-291, (2001)
- [5] S. Y. Lee, NIM-A, 300 (1991), p. 151
- [6] <http://www.ansys.com>
- [7] B. Podobedov et al, to be published